Erosion and Foreign Object Damage of Thermal Barrier Coatings

J. R. Nicholls and R. G Wellman
Cranfield University
Cranfield, Bedford
UK
Tel: +44 1234 754039 / Fax: +44 1234 752473

Email: j.r.nicholls@cranfield.ac.uk

ABSTRACT

Thermal barrier coating are perceived as an enabling technology to increase the performance of, improve efficiency within, and lower the emissions from, modern gas turbines. To fully utilise this capability one has to be able to accurately predict the life of these coatings under conditions relevant to gas turbine service.

This paper addresses the failure of TBC systems as a result of erosion and foreign object damage. Laboratory studies under controlled conditions using a high temperature gas gun rig are reported and compared to damage observed within engines. Models for erosion and foreign object damage have been reviewed and results from these models compared to observed damage mechanisms. The damage mechanisms that result are related to service parameters including temperature, velocity, particle size, impact angle and TBC material properties.

1. INTRODUCTION

The concept of a thermal barrier coatings (TBC) was first introduced some 40 years ago (see [1-4]), whereby a ceramic insulating coating was applied to a cooled metallic component to reduce the metal surface temperature. Two basic process technologies are now widely adopted within gas turbine manufacturing to deposit thermal barrier coatings (TBCs), that is plasma spraying – in vacuum for the bondcoat, or air for the topcoat – or EB-PVD (electron beam physical vapour deposition). The microstructures of these two TBCs are presented in Figures 1a and 1b.

Unfortunately, for high thermal loaded engines plasma sprayed TBCs gave poor early durability and this triggered extensive work aimed at developing strain-tolerant microstructures. The EB-PVD TBC [1-6] and the segmented, thermally sprayed TBCs [7,8] were outcomes of this research. The EB-PVD has proved particularly successful, resulting in significant improvements to coating durability on heavily loaded components as a result of the columnar strain-tolerant microstructure that is developed [5,9-13] EB-PVD TBCs are now specified for aerofoil components within aero-gas turbines and their derived industrial counterparts [5,14]. Flight service evaluation – published in the open literature [9,15] has shown that this class of coating can survive up to 16,000h in a turbine environment.

Paper presented at the RTO AVT Specialists' Meeting on "The Control and Reduction of Wear in Military Platforms", held in Williamsburg, USA, 7-9 June 2003, and published in RTO-MP-AVT-109.

Modern thermal barrier coatings are a multi-material coating system, optimized to protect hot gas components within gas turbines and other high temperature power plant. The coating consists of three important material components:

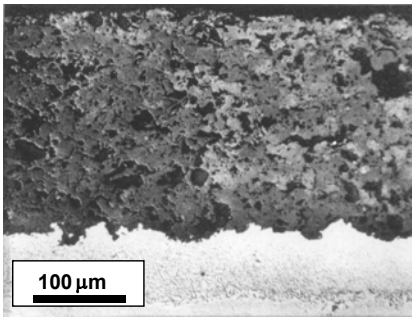

a) Micrograph of a Plasma sprayed TBC

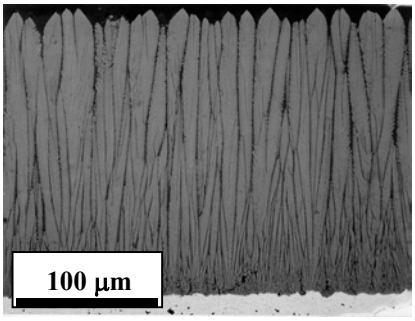

b) Micrograph of an EB-PVD TBC

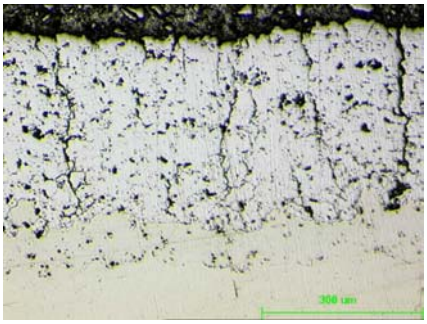

c) Micrograph of a segmented plasma sprayed TBC

Figure 1 Typical ZrO_2-(7-8)wt%Y_2O_3 thermal barrier coating microstructures

An outer ceramic top coat – The most prevalent material is ZrO_2-(7-8)wt%Y_2O_3 (PYSZ), although a number of alternative ceramics have also been considered. Newer materials having lower thermal conductivities include zirconia with multiple rare earth stabilizers [16-19] and pyrochlore phases, such as gadolinium zirconate [19]. Anecdotal evidence suggests that these alternative materials exhibit inferior erosion resistance and a greater susceptibility to delamination than the commercial standard 7YSZ [20,21]. Thus, the challenge in developing new oxide systems with enhanced overall performance is to understand the dichotomy between improved thermal resistance and the ceramics reduced durability [20]. This dichotomy is being addressed in a joint US/EU programme, HIPERCOAT[1], researching high performance thermal barrier coating systems. The issues of erosion and foreign object damage performance will be addressed in this paper.

A bondcoat system: Bondcoats for TBCs include the established MCrAlY series of environmental protection coatings, diffusion aluminides and most recently the γ+γ', platinum diffused single crystal materials [22-25].

The thermally grown oxide (TGO): The mode and rate of growth of the thermally grown oxide is critical to the durability of the TBC system. Since the conception of TBC systems much work has been undertaken to

[1] Joint NSF/European Commission research programme into "Science of High Performance Multifunctional High Temperature Coatings", EU Contract No. GRD2-200-30211.

understand how the alumina oxide grows, interacts, degrades and finally fails during high temperature service, specifically as measured by the thermal cyclic life [26-31]. The multi-material aspects of the TBC system complicate this understanding through, diffusion, stress relaxation and chemical interactions between the component parts.

Until recently, the use of TBCs has been restricted to non-critical applications, however, with the push for greater efficiency, lower emissions and high operating temperatures, TBCs are finding use on load-critical components. Under such conditions, partial ceramic loss could lead to increased operating temperatures and may compromise the integrity of the components being protected. For critical components, where the TBC is being relied upon to deliver the desired engine performance, such loss may lead to rapid TGO growth, enhanced bondcoat degradation (a result of corrosion and interdiffusion), substrate embrittlement and, in limited extreme cases, local melting of the component.

This paper addresses the failure of TBC systems as a result of erosion and foreign object damage. Clearly, the total loss of ceramic, down to the bondcoat/ceramic interface due to ballistic impact – known as foreign object damage (FOD) – can have disastrous consequences in terms of the performance of critically loaded components, such as the HP turbine blades, when the TBC is being relied upon to deliver the desired engine performance.

Erosion arises because inertial forces cause particles, entrained within the gas stream, to deviate away from the gas streamlines, thus impacting the components within the gas flow [32]. Thus small particles (<1-2μm) will generally follow the flow and cause little erosion [32,33]. Particles above 2μm but less than 20μm may impact inclined surfaces, where significant local aerodynamic effects modify particle impact conditions [34]. Thus intermediate sized particles (10-20μm) cause erosion to the trailing edge of turbine aerofoils [35]. Large particles (>40μm) move relatively slowly in the gas stream and can be hit by the rotating turbine hardware damaging the leading edges [14,36-37]. In this latter respect, particulates generated within the engine, such as carbon particles formed within the combustion process [37], and engine wear residues, such as thermally spalled TBC from the combustor [14], can contribute significantly to the observed erosion damage.

Initially perceived as being of secondary importance – when compared to bondcoat oxidation – for static parts, erosion and FOD become more significant for rotating hardware in advanced gas turbine engines. Particularly, the recent observations that the erosion resistance of many of the new lower thermal conductivity TBCs is worse than the commercial 7YSZ materials [21] and that during service the erosion resistance of EB-PVD TBC coated parts can degrade by up to a factor of x4 due to ceramic sintering [38,39].

For life-critical applications, erosion of the ceramic top coat is perceived as a potential problem, whether for aero- [5,10-13,40] or industrial applications [5,14]. Thermal barrier coatings are more susceptible to erosion than fully dense ceramics [41] because the coating microstructures contain many crack-like features – discussed later in section 3.

2. EXPERIMENTAL STUDIES ON THE EROSION OF THERMAL BARRIER COATINGS

Studies into the erosion performance of thermal barrier coatings are somewhat limited in the published literature, with the majority of studies using either the Cincinatti wind tunnel rig, the Cranfield gas gun facility, or industrial burner rig facilities. The capabilities of the two laboratory test facilities were compared in a previous EPRI research workshop into corrosion in advanced power plants (see reference 42).

Experimental studies are roughly evenly split between studies of plasma sprayed systems [1,9,38,40,41,43,46-50] and EB-PVD systems [1,10,14,15,40,43-45], although data on the latter, to a significant degree, have only recently become available. Both laboratories (Cincinnati and Cranfield) have the ability to test at room temperature and elevated temperatures. Tests up to 815°C and 910°C have been undertaken in these test facilities respectively and the experiments undertaken in both facilities when testing coatings to the same manufacturing specification, give similar results [41,47,48]. The difference between the two approaches is that Cincinatti use a combustion based system, burning fossil fuels, to produce the hot gas stream; while Cranfield uses an electrically heated, high velocity gas gun [42].

Comparing results from both of these laboratories, and incorporating the limited experimental data from other laboratories, permits a data set for the erosion of APS (air plasma sprayed) TBCs over the temperature range RT-1600°C and EB-PVD coatings over the temperature range RT-910°C to be established for particle velocities up to circa 300ms^{-1}. Recently limited data on the erosion of segmented, plasma sprayed TBCs is available from tests undertaken as part of the COST522 programme[2].

Trends from this dataset, together with current understanding of the mechanisms of failure under erosion and FOD are discussed in this paper.

Firstly, Figure 2 presents a comparison of the erosion performance of an air plasma sprayed (APS) TBC, with a lamellar microstructure resulting from the deposition of pancake like splat particles, to an EB-PVD TBC with the classic columnar microstructure. Tests on bulk zirconia are included as a reference. Bulk ZrO_2-8wt%Y_2O_3 when eroded with 100µm alumina particles gave erosion rates of 3.6 ± 0.1g/kg at room temperature (particle velocity was 140m/s) and 12.5 ± 2.9 g/kg at 910ºC (particle velocity was 230m/s) [48,51]. Also included in Figure 2 are the more recent erosion studies undertaken on a segmented plasma sprayed microstructure (see Figure 1c), evaluated as part of the COST 522 programme[2].

It can be seen from Figure 2 that at room temperature (20ºC) and 910ºC, the columnar EB-PVD microstructure is more erosion resistant than the splat-like APS microstructure by a factor of approximately x10, under normal (90º) impact conditions. Erosion rates were respectively 20 g/kg (20ºC, 140m/s) and 28.5 g/kg (910ºC, 230m/s) for the EB-PVD columnar microstructure compared to 210 g/kg (20ºC, 140m/s) and 322 g/kg (910ºC, 230m/s), for the splat-like APS microstructure. The vertically microcracked plasma sprayed TBC by comparison – although only tested at room temperature – exhibited erosion rates much closer to that expected for EB-PVD ceramic than APS ceramic, namely 24.4 g/kg (20ºC, 140m/s).

[2] COST 522 Gas Turbine Group – Work Package 2 Protective Systems.

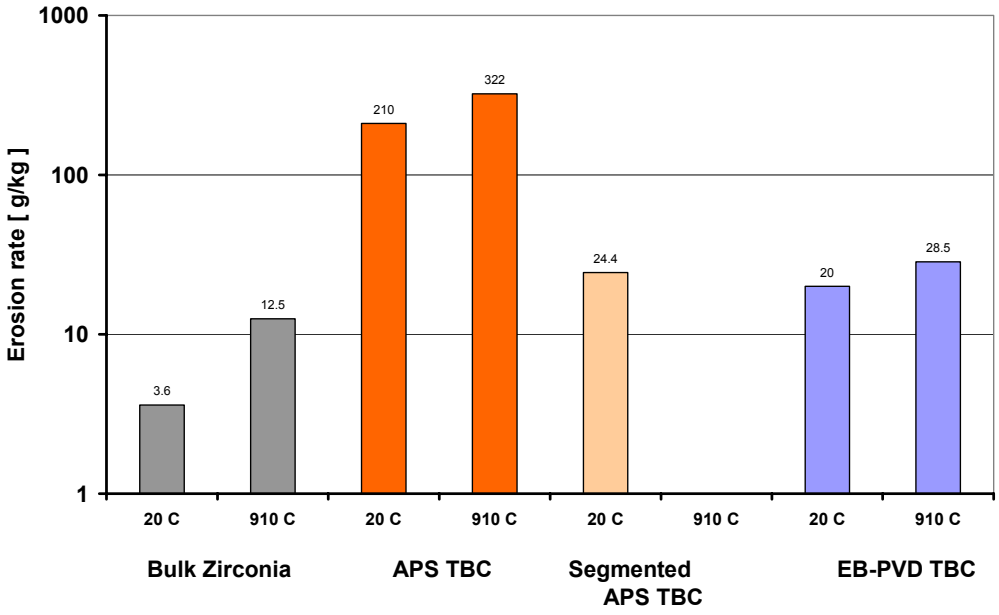

Figure 2 Comparison of the erosion performance of air plasma sprayed, EB-PVD and segmented plasma sprayed coatings at RT and 910ºC. Data for bulk ZrO_2-7wt%Y_2O_3 ceramic is included as a reference

All coating morphologies are significantly less erosion resistant than the bulk ceramic (the EB-PVD ceramic erodes at x 2 to x 5 the rate of bulk zirconia, depending on test temperature), confirming the premis that the crack-like features inherent in the design of successful thermal barriers must compromise the erosion performance. The ability of the columnar boundaries in the EB-PVD ceramic microstructure (and the vertical microcracks in the segmented APS TBC) to limit crack propagation is thought to account for its improved erosion resistance over the conventional air plasma sprayed microstructure.

Recent room temperature erosion studies undertaken at Cranfield under the HIPERCOAT programme on gadolinia doped (2mole%), zirconia-4mole% (7wt%) yttria confirmed the anecdotal evidence that rare earth doped EB-PVD TBCs erode at a higher rate (less erosion resistant) than the industrial standard ZrO_2-7wt% (4 mole%) Y_2O_3 material. The measured erosion rate using 90-125µm alumina, at 90º impact with a particle velocity calculated to be 100-110m/s was 29-34g/kg, 2-3x that of the ZrO_2-7wt%Y_2O_3 material, at 11-13g/kg [52]. Work into the erosion and foreign object damage resistance of advanced TBC compositions is on-going as part of the HIPERCOAT programme. Clearly this dichotomy between improved thermal resistance and reduce damage tolerance must be addressed so that advanced ceramic systems with balanced properties and improved overall performance can be developed.

2.1 Erosion Performance of Commercial EB-PVD Thermal Barrier Coatings Deposited onto Aerofoil Components

At Cranfield repeat EB-PVD TBCs, of commercial manufacture, have been tested using 100µm alumina at 230ms^{-1} and 910°C [41] or 140ms^{-1} at room temperature [48,51]. The aim of this series of tests was to evaluate the repeatability of erosion behaviour from sample to sample (using 25mm x 25mm test pieces) and by location around a coated blade (samples were cut from the suction surfaces, pressure surface and from the

leading edge). The repeatability of the test pieces reflects the reproducibility of the coating process from one run to another, while the repeatability of samples taken from a blade reflects the reproducibility of manufactured around a blade profile.

Measured erosion rates on test pieces (TBC thickness 360µm), when tested at 90º impact and 910ºC using 100µm alumina at a velocity of 230m/s, varied between 14.0 and 28.5g/kg with a mean of 19.8g/kg. The data, see Figure 3, was found to fit a classical Weibull model, when plotted as erosion resistance (1/erosion rate) where F_w is the Weibull probability, E is the erosion rate, E_o is a minimum erosion rate under these test conditions and β, η are constants.

This is to be expected for fracture behaviour controlled by the size of inherent defects. The Weibull model was of the form:

$$F_w = 1 - \exp\left\{\frac{\left(1/E - 1/E_o\right)^{\beta}}{\eta}\right\}$$

Where the Weibull modulus β takes a value of 3.6 for batch to batch variations in EB-PVD TBC manufacture. The characteristic erosion resistance (η) for this data set is 0.060 kg/g (corresponding to a characteristic erosion rate of 16.8 g/kg).

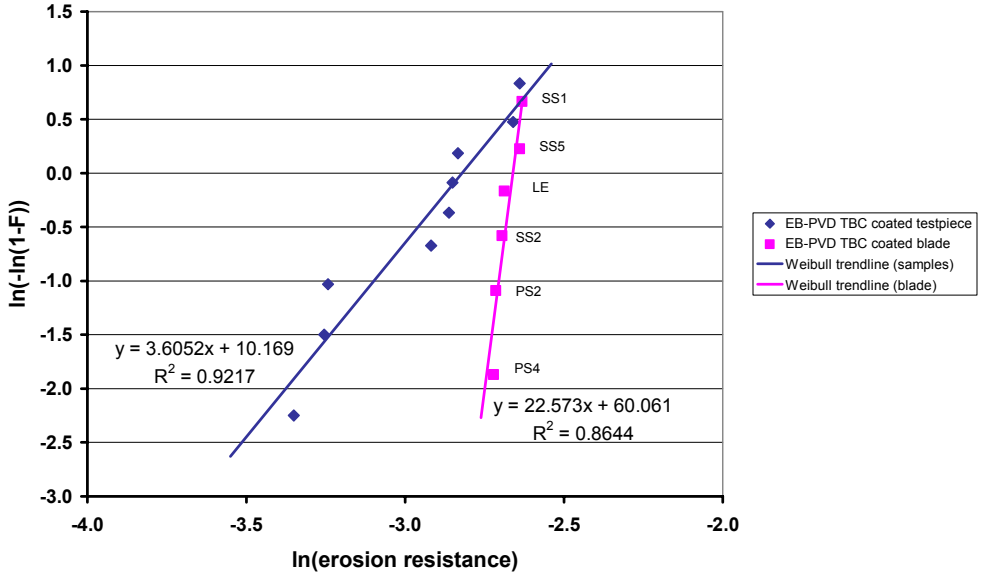

Figure 3 Weibull analysis of the repeatability of erosion data for EB-PVD thermal barrier coatings tested at 910°C [Included in this figure is data taken from Figure 4 on a blade sample, which represents the most likely within batch variation: Note: the R^2 values quoted on the figure are a measure of the 'goodness of fit'; an R^2 value of 1.0 is a perfect fit to the data].

TBC coated blade samples, courtesy of CUK Ltd, were provided as a through blade section cut from an industrial turbine blade, coated with RT33 ZrO_2-8wt%Y_2O_3, EB-PVD ceramic. Each segment tested was 25mm x 25mm area approx. with 10 segments taken around the blade profile (label SS1 to SS5 along the suction surface, LE leading edge and PS1 to PS4 along the pressure surface). Six of these samples have been erosion tested at 90º impact at room temperature, using 100µm alumina at a velocity of 140m/s. Figure 4 plots the result of this study, effectively mapping the erosion rate of the EB-PVD TBC around the blade profile. Erosion rates varied around the blade profile, from 13.9 g/kg on the pressure surface (PS4) to 14.8 g/kg on the leading edge (LE) and a maximum of 15.2 on the suction surface (SS1). This trend maps out the degree of constraint around the blade for on the suction surface the coating grows into a more open space (convex surface), while on the pressure surface the space is constrained (a concave surface). These growth constraints will modify the EB-PVD column size and the extent of intra-column porosity, thus influencing the erosion rate.

Whilst discussing constraints introduced by blade geometries another factor that must be taken into account is the likelihood of producing inclined column microstructures during the manufacture of EB-PVD TBC coated turbine parts. Areas prone to these, non-ideal microstructures are the shrouds and platforms of the HP turbine blades and the deposition into the intra-vane spacing for nozzle-guide vane pairs Inclined columns on platforms and shrouds can be partially alleviated by applying a butterfly action to the blade manipulators during TBC deposition. However, such remedial actions are not possible when considering the constraints offered by nozzle guide vane pairs. Here the column inclination is defined by the incident angle of the vapour flux and the available aperture between the pair of nozzle guide vanes.

Good erosion resistance of EB-PVD thermal barrier coatings requires that the columnar microstructure is vertically aligned. Any off axis symmetry modifies the mode of column fracture and this has a significant effect on the erosion rate. Figure 5 illustrates the increase in erosion damage that can occur when the TBC growth direction is inclined. On impact, fracture may occur throughout the coating (rather than in the near surface region as discussed in the next section for a vertically aligned EB-PVD TBC microstructure) with some fracture at mid-column length and others near to the bond coat surface. This behaviour is believed to result from bending of the columns during impact, such that the largest defect in the column surface causes fracture.

Clearly, the TBC microstructure, developed as part of the manufacturing process can have a major effect on erosion behaviour. This effect of column inclination would be significant when coating such components as nozzle guide vanes, which are often designed with multiple aerofoil parts. At shallow angles of inclination <7.5°, erosion rates in excess of 6,000 g/kg are observed (see Figure 5). In fact, the EB-PVD TBC performs worse than an APS TBC when the columns are inclined at angles below 50°. For acceptable performance it is recommended that off axis inclination be kept less than 15º (i.e. inclinations between 75-90º). This would give a doubling of the erosion rate.

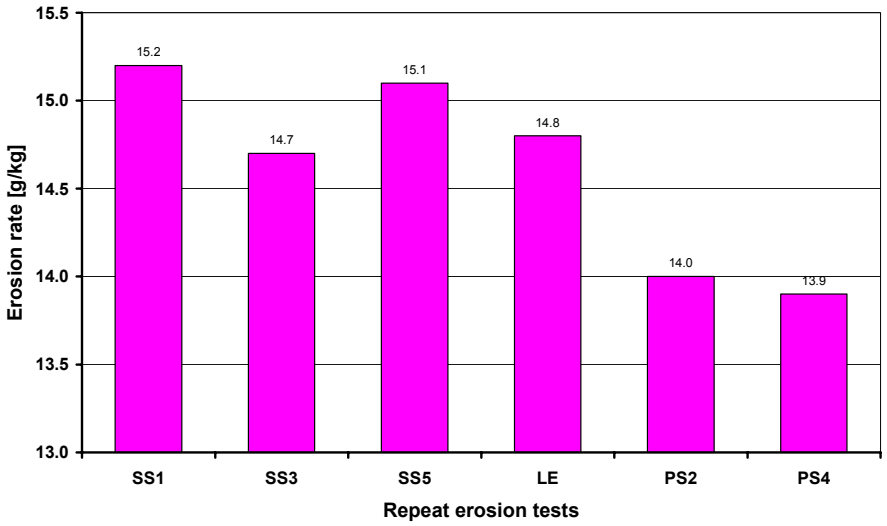

Figure 4 Variation in erosion rate of a commercial EB-PVD TBC (RT33) around a blade profile.

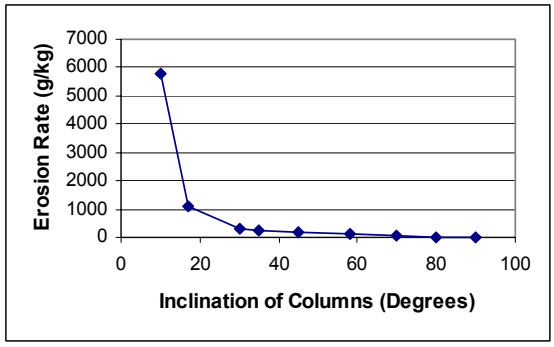

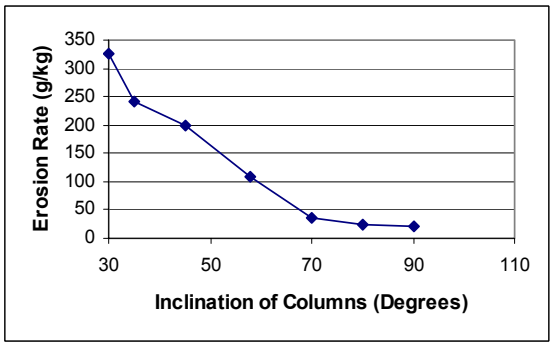

a) Column inclination 7º to 90º b) Enlargement of region 30º to 90º

Figure 5 Influence of column inclination on the erosion rate of EB-PVD TBCs

3.0 OBSERVED DAMAGE MECHANISMS IN THE EROSION AND FOREIGN OBJECT DAMAGE OF EB-PVD TBCS [38,39,41,47-51].

It has been demonstrated in the previous section that EB-PVD TBCs are inherently more erosion resistant than their air plasma sprayed counterpart. Factors between x7 and x10 have been reported depending on the exact test conditions and ceramic microstructure developed in coating manufacture. This section discusses the material removal mechanisms and the role of microstructure.

The difference in erosion behaviour is associated with the differing modes of failure for an air plasma sprayed (APS) and EB-PVD coatings. The APS coating fails by the propagation of cracks along splat boundaries and through the microcrack network that are an inherent part of the microstructure and which provide some degree

of strain tolerance [41]. In contrast, the EB-PVD coating when impacted by particles of 100µm or less forms parallel, near surface cracks within the columns [47-49]. Cracks stop at column boundaries, see Figure 6, and a number of neighbouring columns need to fracture before material is lost.

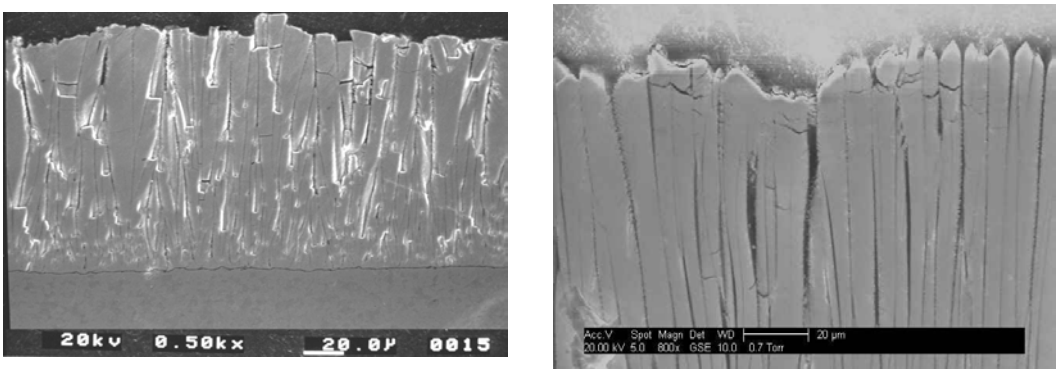

(a) Room Temperature (b) 800ºC

Figure 6 Cross sections of eroded samples of TBCs showing near surface cracking, a) at room temperature and b) at 800ºC

The mechanism of foreign object damage (FOD) is more complicated and involves gross plastic damage and shear bands within the TBC [10,21,39,47,51] often leading to cracks down to the metal oxide interface and thus large scale ceramic removal (see Figures 8a)-c) later in this paper).

In the following sections, the different erosion and FOD mechanisms will now be discussed and defined according to the observed damage for the different impact conditions starting with low energy impacts. The authors define erosion as the loss of material from the top 5-20µm of the coating through repeated impact by small particles causing near surface cracking in individual columns. FOD involves gross plastic damage, the bending of columns and ultimately the propagation of shear bands down to the ceramic bond coat interface.

3.1 Mode I - Erosion (Near surface cracking/lateral cracking)

Erosion is the standard term used by most authors in the literature to describe the progressive loss of material from the surface of an EB PVD TBC while still maintaining the integrity of the columnar microstructure. This occurs under small particle impact conditions where the near surface region, the top 20µm, of the individual columns are cracked due impact. Material is lost when a number of neighbouring columns have been impacted and cracked. The cracks are observed to initiate at the elastic/plastic interface that occurs under the impacting particles [38,39], this type of damage is illustrated in Figure 6.

The relevance of room temperature erosion testing has been questioned as to whether it is representative of high temperature erosion. As far as can be seen from Figure 6a and 6b the same mechanism of near surface cracking occurs at both room and high temperatures. Although, it can be argued that the degree of plastic deformation that can be accommodated by the ceramic at elevated temperatures is greater than at room temperature. However, analysis of samples eroded at both room temperature and high temperature showed that there was no difference in the observed depth at which the near surface cracking occurred during Mode I erosion of the samples.

Erosion rates are highly dependent on a number of material properties which include Young's Modulus, Hardness and Fracture Toughness, all of which are affected by temperature. Thus, it can be argued that although the erosion mechanism at room temperature and high temperature is nominally similar the erosion rates could well be different.

3.2 Mode II - Compaction Damage

This is a relatively new observation and is essentially a transition mechanism that occurs between erosion and FOD. It involves the compaction of the columns without the cracking that occurs during erosion or the gross deformation of the columns that occurs during FOD. This type of damage has been observed under both room temperature and high temperature impact conditions, and is illustrated in Figure 7. Figure 7, a room temperature impact, illustrates the ability of EB PVD TBCs to deform plastically, even at room temperature. Note however, that this type of plastic deformation, as in Mode I erosion, is most likely in the form of the densification of the near surface individual columns. Penetration depths are expected to be greater than under Mode I erosion with the higher impact energies involved in Mode II compaction.

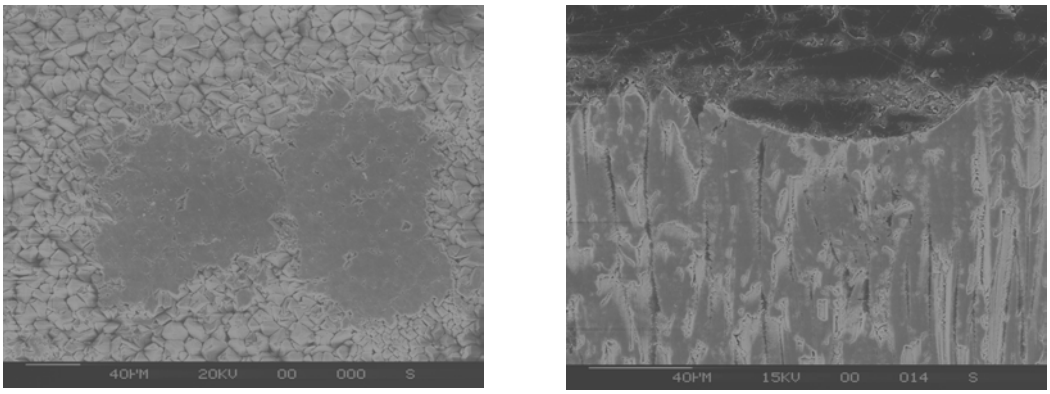

(a) (b)

Figure 7 Micrographs of single impact Mode II compaction damage showing compaction of the coating, note the absence of cracking, a) top view, b) cross section. [200µm particle impact, at 170m/s at room temperature]

Thus, in this intermediate/transition damage mechanism there is compaction of the EB PVD TBC columns, but neither the near surface cracking of Mode I nor the gross plastic deformation, kinking and cracking of Mode III is observed. This compaction damage is attributed to the high porosity levels in the columns, which are never 100% dense, often containing up to 15% of nano-sized porosity together with intra-column pores. A similar type of compaction occurs during Mode I, here the damage is limited to one or two neighbouring columns, with any lateral cracks believed also to initiate from the elastic/plastic interface. However, when the impact is spread over a significant number of columns, as is Mode II compaction damage, cracks do not initiate at this interface thus the transient loads on each column must be lower, below the fracture stress of the individual columns. This type of damage is observed for larger particles travelling at intermediate velocities and is thought to be due to a lower rate of energy input by the decelerating particle.

This mechanism is still under investigation but it is evident from the initial single impact studies that the Mode II damage mechanism is different form the other two and that cracking does not occur under single

impacts. Multiple impacts studies are underway to determine the exact mechanism that is operating under Mode II conditions, which may well be a form of impact fatigue damage.

3.3 Mode III - Foreign Object Damage (FOD)

FOD is caused by large particles travelling at low velocities or smaller particles at higher velocities and is characterised by significant deformation of the coating which can penetrate to the substrate and is accompanied by gross plasticity, deformation of the columns, shear bands and extensive cracking of the TBC ceramic [10,21,47,48,53,54] as illustrated in Figure 8. Clearly, the extent of gross plasticity observed varies with the component temperature when impacted, being greatest at 1200ºC and less prevalent at room temperature.

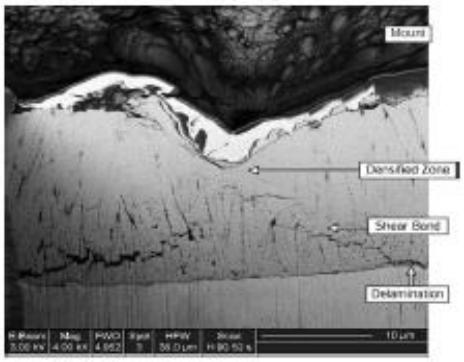

(a) 1200ºC

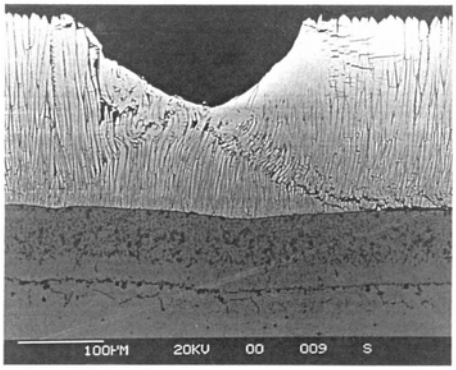

(b) 900ºC

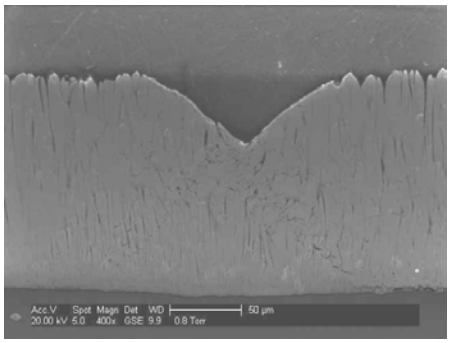

(c) 800ºC

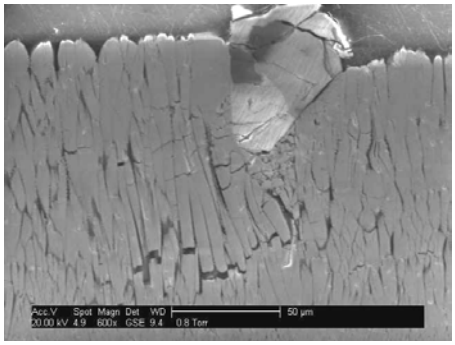

(d) R.T.

Figure 8 Micrographs illustrating the effect of FOD in an EB PVD TBC, a) damage at 1200ºC [21,55], b) damage at 900ºC [1mm spherical alumina particle at an estimate 100m/s] [10] c) 800ºC [39] d) damage at room temperature [0.5mm angular alumina particle at an estimated 100m/s] [39]

Further, recent studies have shown that, in fact, there are a number of distinct types of FOD. The SEM micrograph in Figure 9 illustrate an additional form of FOD damage – termed type 2 FOD – where significant column buckling is observed. This mode was observed in high velocity, gas gun FOD tests at Cranfield and demonstrates that EB PVD TBCs can deform plastically at elevated temperatures, in this case 800°C.

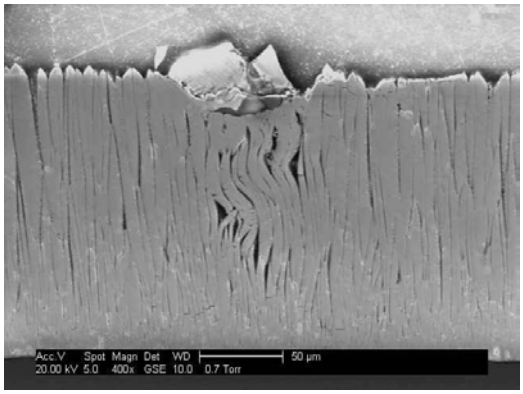

Figure 9 SEM micrograph illustrating type 2 FOD in EB PVD TBCs impacted at 800°C [39]

From these studies it appears that an additional type of foreign object damage can occur that involves significant buckling of the columns and plastic deformation without noticeable cracking. It is expected that subsequent impacts would increase the degree of buckling in the columns until cracking initiated and material was lost. FOD Type 1 is the standard accepted mechanism of gross plastic deformation of the coating with the associated densification bending and cracking of the columns as shown in Figure 8 a-c. Thus, foreign object damage has been observed to give rise to three distinct damage morphologies, mechanisms each of which can be summarized as follows:

3.3.1) Type 1 FOD

Type 1 FOD may give rise to either of two damage morphologies. These morphologies result from essentially the same mechanism, differing only in the relative degree of cracking and plastic deformation that occurs, which is a direct result of the temperature of impact. As can be seen in Figure 8a – 8c (1200°C, 900ºC and 800ºC) Type 1a FOD exhibits a significantly greater degree of plastic deformation under the impact. Gross plastic deformation of the coating is in the form of compaction damage immediately below the impact with associated bending and cracking of the columns to form lateral shear bands propagating down to the ceramic/substrate interface. Type 1b FOD (room temperature) exhibits noticeably less gross plasticity (Figure 8d) instead there is a significant amount of cracking observed in the columns of the sample due to the more brittle nature of the ceramic columns at room temperature.

It is under conditions of FOD that the effect of temperature becomes most noticeable in that the mode of damage is directly affected by the temperature at which the impact occurs. After room temperature impact the columns are still visible as discreet features, whereas as the temperature increases, impact conditions result in the coating densifing as a whole. In other words the impact has caused adjacent columns to compact together so that they are no longer discreet columns.

3.3.2 Type 2 FOD

This mode of damage has only recently been observed in high temperature laboratory tests [39] and demonstrates the ability of EB PVD TBCs to deform plastically without densification occurring. As can be seen from Figure 9 the impacting particle has caused a number of columns in the coating to buckle with virtually no cracking occurring. From these experiments [39] this mode of deformation can be expected to occur at temperatures in excess of 800°C (being the temperature at which these tests were conducted) and possibly lower temperatures as well, provided the ceramic material exhibits sufficient plasticity.

Both Type 1 and Type 2 FOD was found to occur in the same sample and are thus *not* mutually exclusive mechanisms. Which mode of damage occurs can be assumed to depend on the local impact conditions, and the constraint between neighbouring TBC columns.

4.0 MODELS FOR THE EROSION OF THERMAL BARRIER COATINGS

Recent work within the HIPERCOAT programme has focused on understanding the material removal mechanisms for an EB-PVD thermal barrier coating system under the wide range of impact conditions that may be envisaged in a gas turbine, as depicted in the micrographs in section 3 of this paper. These modeling studies have involved a collaboration between researchers at Cambridge [55,56], Santa Barbara [21, 53-55] and Cranfield [39, 48-52, 57], where Cranfield have provided much of the experimental evidence of the damage incurred. Cambridge has modeled the dynamics of particle impaction, examining in particular the evolution, propagation and dissipation of energy from the elastic stress wave during impaction. Work at Santa Barbara has focused on elasto-plastic interactions during large particle impact (FOD), by utilizing a high temperature indentation system to examine the flow characteristics of the TBC under indentation load.. They have developed F.E. models of the TBC system and compared the models to damage produced using depth sensing, spherical indentation, at temperature [21, 53-55]. Figure 10 illustrates schematically these two modes of damage. Figure 10a is representative of coating failure during small particle erosion due to the propagation of elastic stress waves down the columns of an EB-PVD TBC. Figure 10b illustrates the gross plastic damage and shear banding that results from foreign object damage (FOD).

Modelling work at Cranfield [29-31] has focused on understanding the material removal mechanisms, and thus the development of a Monté Carlo model to predict EB-PVD TBC erosion rates, whilst operating in the Mode I (small particle impact) damage regime. In support of this modeling work, and to provide indentation data (and mechanical properties) for individual columns and small clusters of columns, nano- and micro-indentation studies of the EB-PVD columnar structure have been undertaken [58] complimenting the macro-indentation studies of Santa Barbara. Each of these modeling activities will now briefly be reviewed, in light of the experimentally observed damage.

4.1 The Dynamics of Small Particle Impaction [55]

Work at Cambridge University, by Fleck and co-workers [55,56] has examined the loading deformation and fracture events during dynamic indentation of an EB-PVD TBC microstructure. Figure 10a schematically illustrates the problem. On impact an elastic stress wave propagates down the column, the wave can reflect from the coating/substrate interface or from internal defects within the columnar microstructure. The edge of each column is assumed to contain incipient cracks – the porous, dendrite like structures that result from the EB-PVD process, during TBC manufacture. This modelling work at Cambridge aims to address how these stress waves interact with the coating, the position of any peak stress that are generated and whether they are sufficient to cause fracture of the columns.

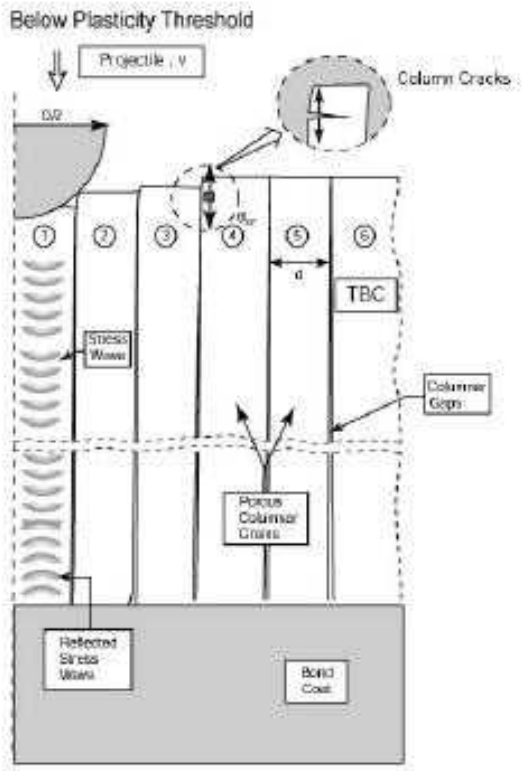

a) Small particle impact - elastic impact between a spherical projectile and a plastic damage as a result of columnar microstructured ceramic

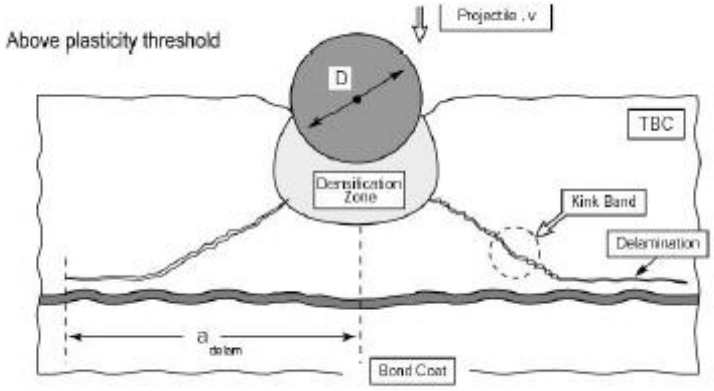

b) Large particle impact elasto-coating FOD

Figure 10 Schematic diagrams of particle impact dynamics on an EB-PVD TBC [55,56]

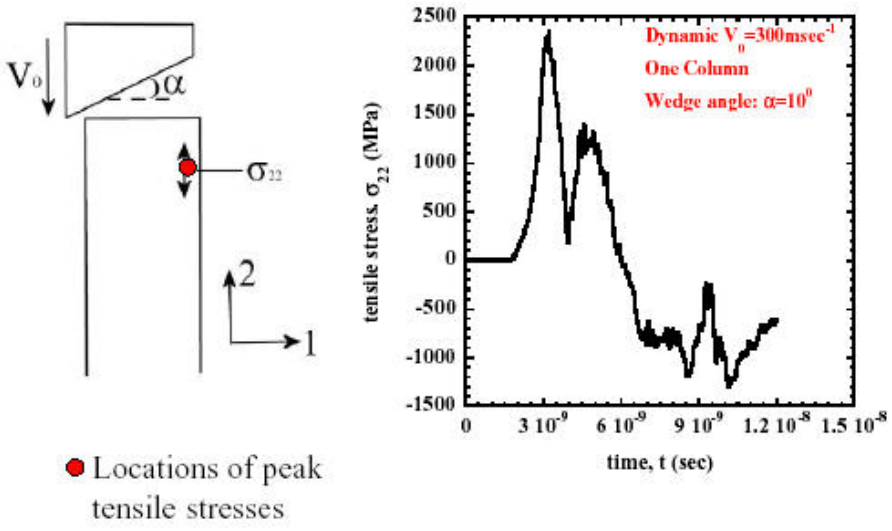

Figure 11 Wedge impact model of particle/TBC dynamics [56]

With further penetration, the columns may elastically bend, leading to fracture, in a mode similar to that observed under quasi-static indentation. This local elastic bending would depend on the column length to diameter and the local constraint from neighbouring columns.

Such elastic flexture and cracking can absorb impact energy, however, for large particles at sufficiently high velocities impact conditions may exceed yield then local plastic deformation can occur further adsorbing the energy of the impact. Plasticity is first seen as a densification of the near surface layers (observed in experimental studies of small particle impacts). This progresses to the observed compaction damage and ultimately leads to the complex failure conditions observed in foreign object damage, where kinking and lateral cracking are observed as well as gross plasticity. The question is "under what conditions do each of these modes of damage occur?"

Considering first the elastic stress wave, the impact conditions can be simplified to a simple wedge impact problem, which can be analysed using finite element analysis. Figure 11 illustrates this model and the predicted tensile stress (σ_{22}) as a function of the elaped time from impact. At an impact velocity of 300m/s and a wedge angle of $\alpha=10^{o}$ (α represents the contact angle between the impacting particle and a particular column) a peak stress of 2.5 GPa is calculated. The elapsed time to this peak stress condition is just greater than 3ns, which corresponds to the onset of cracking 10μm from the top of the column [55,56].

This behaviour is in broad agreement for damage observed during small particle impaction – Mode I. The observation of local, near surface plasticity, under high temperature impact must modify this analysis somewhat. It is expected that the change in density between the compact surface region and the remainder of the column may act to concentrate the stress peak intensity, resulting in fracture preferentially in this region.

4.2 Plastic Indentation, Compaction Damage and the Generation of Shear Bands under Large Particle Impaction

As shown in Figures 6, 7 and 8, local densification of the near surface under impact is central to all erosion and FOD events at high temperature. Whether this is true plastic damage or the removal of inherent nano- and intra-column porosity by dynamic compaction as a result of repeated impacts is still open to conjecture. However, it is now widely accepted [39, 49-51, 53,55] that the formation of this surface densified zone is an important step in the erosion or foreign object damage to TBCs. This aspect has been modelled, and studied experimentally by A. G. Evans and co workers [21, 53-55] at Santa Barbara in California, USA, as part of the joint EU/US HIPERCOAT programme

It is clear, that when large particles impact with high momentum at high temperature most of the kinetic energy is adsorbed by plastic deformation and densification of the TBC (see Figures 7 and 8). The deformation may be accompanied by kink bands around the perimeter of the plastic zone, [10, 21, 39, 51] which, if present, propagate to the TGO (thermally grown oxide) and initiate delamination cracks. A schematic diagram for a model of this mode of damage is illustrated in Figure 12 [55] which compares well with experimentally observed damage at high temperatures (see Figures 8a-c). Even for multiple small impacts, at temperature a near surface densified zone is observed.

The finite element model, proposed by Evans and coworkers [53] is axisymmetric (Figure 12), with the columnar microstructure approximated by a series of concentric cylinders, with gaps between each cylinder. Thus, the role of contact between columns can be explored by varying the properties of this intra-column region [53,55]. As part of this modelling work, Evans and co-workers have identified a number of important dimensionless groups and have examined the relationship between them. The impact energy can be normalized [54,55,59] as:

$$\Omega = \left(\pi/12\right)\left[\rho_P / \sigma_y^{tbc}(0)\right] V^2$$

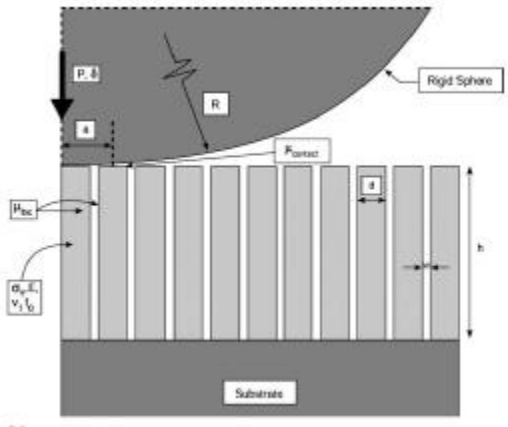

Figure 12 Schematic model for indentation of an EB-PVD microstructure [53]

The maximum penetration of a projectile into the TBC ceramic microstructure (δ_{max}) depends on the porosity. Assuming a porosity of 20%, the result is [54].

$$\frac{\delta_{max}}{D} = 0.38\sqrt{\Omega}(0.1 + 0.84\sqrt{\Omega})$$

with the depth of the densified zone $(h_D) \approx 4\sqrt{\delta_{max} D}$

where D is the particle diameter, ρ_p the density of the particle, $\sigma_y^{tbc}(0)$ is the flow stress of the TBC measured form static indentation tests (low flow rates) and V is the velocity of the impacting projectile.

This plastic zone induces residual stresses that scale with $\sigma_y^{tbc}(0)$, but having peak values much smaller than those caused by elastic stress wave propagation, early in the impact sequence [55]. However, when the plastic zone penetrates deep into the TBC, the large special displacements generate stress fields that are very damaging due to the formation of kink bands and large scale delamination. Figure 13 illustrates the predicted plastic deformation following high temperature ball indentation, aimed at simulating the damage mechanism during FOD [21,53]. These F.E. studies have shown that the shape and size of the plastic zone that develops is strongly dependent on both the contact friction and intracolumn friction that is developed during the indentation event.

Calculations of the time dependent change in the stress state acting on the TBC columns, shows that on initial impact an elastic stress wave is generated producing a peak tensile stress, in columns neighbouring the centre of impact. For example, in the 4th neighbour column the peak stress may be as high as 5.6 GPa at a depth of 15µm below the surface [55]. This observations agrees well with experiment, where measured near surface cracks are observed in a range 5-30µm below the TBC surface under small particle – Mode I – impact conditions [38,50,51]. The time for these elastic stress events to occur is of the order 15-20ns.

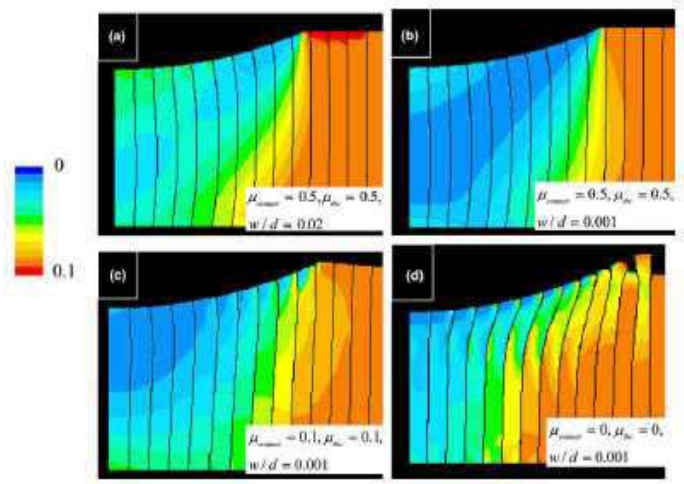

Figure 13 Trends in column deformation and densification as a function of contact friction and intra-column friction [53]

With plastic deformation in the near surface region, the largest normal stress is observed on the third column and for a 5µm dense layer reaches a value of 8 GPa. This normal stress scales with the dense layer

thickness, reducing in value as the layer thickens, approximately $\sigma_{22} \approx {}^{1}\!/\!_{h_D}$. These elastic/plastic interactions occur in timescales of 80-100ns [55].

For large particle impact, delamination and cracking within the TBC is largely driven by the residual stresses that are generated [54]. Such stresses have been analysed by Evans and co-workers using static indentation [21, 60 ,61]. Two basic observations may be concluded: Firstly, when the impact conditions are such that the plastic zone is confined within the TBC, a threshold condition exists, and must be exceeded before cracks can form [62]

$$\frac{\sigma_y^{th}\left(\delta_{max.,}D\right)^{1/4}}{\sqrt{E_{tbc}\Gamma_{tbc}}}$$

This also suggests that based on the yield strength of the TBC at 1150ºC and an estimate of its mode I toughness [55] penetrations as deep as 25μm should be possible without cracking. Such behaviour is consistent with the experimentally observed "compaction damage" regime – mode II – as illustrated in Figure 7.

However, when the plastic zone extends through the TBC and interacts with the TBC/TGO interface, then delamination cracks may nucleate at kink bands and extend just above the TGO. Once nucleated the extension of these cracks will depend on the material properties of the TBC. Evans and co-workers have calculated from their finite element models [54,55] that:

$$\frac{a_{delam}}{H_{tbc}} \approx \left[\frac{(\sigma_y^{tbc})^2 H_{tbc}}{E_{tbc}\Gamma_{tbc}}\right]\left[\frac{\sigma_y^{tbc}}{E_{tbc}}\right]^{\alpha}\left[\frac{\rho_p V^2}{\sigma_y^{tbc}}\right]^{\beta}$$

where $\alpha \approx 1$ and $\beta \approx 1/4$ and H_{tbc} is the thickness of the ZrO_2-8wt%Y_2O_3 (PYSZ) ceramic.

This analysis would suggest that the extent of delamination damage that may result following impact by a foreign object (FOD) varies with the thickness of the TBC and decreases with lower yield stress and higher toughness ceramic materials.

4.3 Monté Carlo Modelling of Small Particle Erosion

Monté Carlo modeling of small particle erosion has been undertaken at Cranfield [38,50,51]. To facilitate this model the microstructure of an EB-PVD TBC is approximated as an array of hexagonal columns, thus each column has six nearest neighbours. The model comprises of 43 columns that 'wrap around' such that columns on the left edge become nearest neighbours to columns on the right etc [31]. A grid of 43 cells is sufficiently large to cover cases where an impacting particle may impact more than one column, whilst small enough to permit rapid calculation of erosion rates and still provide statistical distributions as to the rates of material removal.

The model is a combination of a mechanistic and continuum model as some elements of the model have been derived from a mechanistic understanding of the failure of EB-PVD TBC in the Mode I damage regime

[38,49,50] while other elements are calculated based on continuum mechanics models for bulk ceramics, modified to take into account the unique EB-PVD TBC microstructure. The Monté Carlo model assumes:

1) that during Mode I impact damage near surface cracking develops at depths up to 30μm

2) the majority of cracks are at depths of 6-10μm

3) a critical energy density is necessary to initiate cracking (i.e. a critical velocity + fractional load)

The threshold load for lateral cracking used in this current study follows that calculated by Verspui et al [63] and is given by:

$$P_O = \frac{1200}{(0.75)^2}(\tan\psi)^{\frac{-2}{3}}\frac{E}{H}\left(\frac{K_c}{H}\right)^3$$

where E, H and K_c are the Young's Modulus, hardness and fracture toughness of the target. The depth of the lateral crack is taken to be the depth of the plastic zone (b), which is given by:

$$b = a\sqrt{2}\sqrt{E/H}\left(\frac{\sin\psi}{\cos\psi}\right)^{\frac{1}{3}}$$

where *a* is a measure of the indentation size and ψ is half the included angle of the indenter. To calculate the threshold load for lateral cracking and the depth of the plastic zone, values of E, H and K_c for the EB-PVD coating are required. E and H were measured in this study using the nano-indenter at Cranfield [58]. It can be shown [64] that the indentation volume, the volume of the indenter that penetrates the substrate, determines the global stress field around the indenter. If one assumes the indented volume to be hemispherical, the shape is not important for the stress fields outside the plastic zone, Hill's [65] inflated hole theory can be used to give a relationship between the indent size and the size of the plastic zone. Approximating this relationship by a power law gives:

$$\frac{b}{a} = \mu\left(\frac{E}{H}\right)^m$$

where μ and m are fitted constants (taken as 0.63 and 0.5 respectively), E and H are the Young's modulus and Hardness of the substrate respectively (the EB-PVD TBC in this case) while 'b' and 'a' are respectively the radius of the plastic zone and the indented volume. Thus from knowledge of the EB-PVD coating hardness and modulus (measured using the nano-indenter) the depth of the plastic zone following impact can be estimated for the zirconia EB-PVD TBC.

The radius of the plastic zone, b, can be expressed as: $b = \left(\frac{3mV^2}{4\pi H}\right)^{\frac{1}{3}}\left(\mu\left(\frac{E}{H}\right)^m\right)$

Thus it is possible to determine the depth at which lateral cracking will occur, Z(max), should the impacting particle supply sufficient force to initiate lateral cracking. This cracking occurs at the boundary between elastic and plastic behaviour due to the tensile stresses developed in this region as a result of the propagation of an elastic stress wave down the TBC column and its interaction with microstructural defects introduced as a result of the impact process, or already existing in the coating. If this critical defect is the depth of the plastic zone, then z(max)=b.

To reiterate, the model is a combination of a mechanistic and continuum model in that some of the elements of the model are calculated while other elements are taken from observed results from experimental data. The model is designed to calculate the erosive wear rate of EB-PVD TBCs under various impact conditions and takes into account the stochastic nature of the erosion process by permitting distributions for particle size, particle velocity and coating properties to be introduced.

In order to keep the run time of the programme to a minimum, the model generates a table of values for each random variable and then uses the values to calculate the erosion rate. The lookup table is used to calculate a number of key values for a random selection of 1000 impacting particles, these include contact area, size of the plastic zone and maximum impact force.

Once the lookup table has been completed, the programme picks a random particle from the table then randomly picks a column to impact and a position on the column to impact. This allows the model to determine the percentage of the impact that will be absorbed by the impacted column and its first and second order neighbours. Then it determines whether the columns are already cracked; if not, it will calculate the depth of the possible lateral crack, having checked that the impact force was sufficient to cause cracking, first for the impacted column and its then first and second order neighbours. After each impact the programme then checks whether any column and its first order neighbours have all been cracked and if they have, sums up the material above the crack and adds it to the total of the mass of material removed. It then resets the columns as not cracked and picks another random particle from the lookup table. This process is continued until a pre-specified mass of erodent has been used.

4.4. Validation of Prediction of the Monté Carlo Erosion Model

The model has been run under the same conditions as a selection of the experimental tests. The examples cited here use silica (with an average radius of 30μm) as the erodent at a velocity of 170 m/s at room temperature. As can be seen from Table 1 there is a good correlation between the predicted erosion rates and the measured erosion rates (measured data taken from reference 47).

As one further example, the literature reports a linear increase in erosion rate with velocity in the 100 to 300 m/s velocity range. Experimental studies at Cranfield also support this, showing that E = cV, where c is 0.102 for silica at room temperature and c is 0.131 for angular alumina particle, also at room temperature. [47,48]. The predicted erosion rates are also almost linear in this region with a value for c of 0.13. The degree of fit is apparent from Figure 14.

Table 1: Table of results of Model compared to results from the literature. [*Acknowledged by the authors as an unusually high result, due to spallation loss of ceramic].

Impact Angle (°)	Erosion Rate (g/kg) From Model	Erosion Rate (g/kg) From Literature [47]
90	19.0	17.5
75	18.3	19.5
60	16.1	13.8
45	12.8	31.2*
30	8.7	10

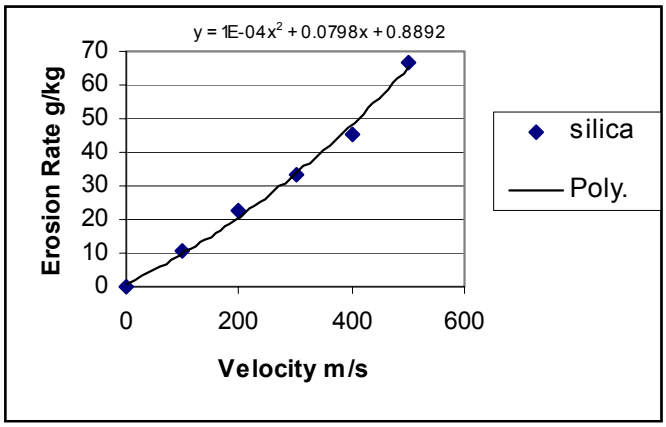

Figure 14: Predicted erosion rate of EB-PVD TBC eroded with Silica at room temperature.

5.0 AN EXPERIMENTAL EROSION MAP FOR AN EB-PVD THERMAL BARRIER COATINGS

Using the Monté Carlo model [49-51] that has been derived to simulate small particle erosion damage to EB-PVD TBCs, erosion rates of EB-PVD TBCs can be predicted. The modelled erosion mechanism assumes near surface plasticity within individual columns which leads to lateral cracking across the columns stopping at column boundaries. No gross deformation of the coating is anticipated as the model aims to predict erosion in the small particle – Mode I – regime. However, as one increases the particle size, or velocity, one would expect the depth and extent of damage to increase, ultimately resulting in large particle compaction damage, and ultimately, foreign object damage (FOD). Thus one must ask "How small, and under what impact conditions does small particle erosion operate, and when does the mechanism transition to compaction damage and then foreign object damage (FOD) occur?"

Erosion maps are an excellent way to visualise these changes in damage mechanisms and thus determine system operating conditions for a particular damage regime. Experimental studies (section 3.0) help in the

evaluation of these boundary conditions. Figure 6 clearly shows Mode I damage, involving lateral cracking across columns. Figure 7 illustrates a more severe condition with plastic damage extending across columns, termed Mode II compaction, while in the extreme, foreign object damage (FOD), Figure 8, can lead to gross plasticity in the EB-PVD top-coat, shear cracking through to the ceramic top-coat/bond-coat interface and possible plastic damage to the bond-coat for the most severe impact conditions.

Figure 15 [57] illustrates an erosion map deduced for impact damage to an EB-PVD TBC, eroded with silica particles. In deriving this map from experimental data, there are three important factors to note. Firstly, the transition velocity from elastic to elastic - plastic damage is assumed independent of particle size, but is dependent on the particle shape. Thus the term (r/R) in the map relates the effective particle radius (r) to the mass average particle radius (R) and included on the map are three positions for this elastic/plastic transition, depending on the (r/R) ratio, plotted for (r/R) ratios of 0.4, 0.6 and 1.0.

Secondly, the critical velocity for lateral cracking is assumed independent of particle shape but is expected to be dependent on the velocity of the impacting particle (left inclined line in the plot).

Thirdly, experimental observations (Figures 6 to 8) show that at increased particle size a transition from near surface plastic damage (mode I) to plastic damage within the TBC (mode II compaction), to foreign object damage occurs, thus two upper bounds (the chain dotted lines to the middle and right of the diagram) can be drawn marking the limit of erosion damage to the TBC and the onset of compact damage, then foreign object damage (FOD).

Finally, the area labeled ‘A’ is of interest. It is a region of the map where near surface plastic damage should occur, but without lateral cracks initiating. One can hypothesis that in this region, material could be removed by some “accumulation of plastic damage” although this has not been incorporated in the current version of the Monté Carlo model. For the model to be valid in this region it would be necessary to accumulate strain, when columns are impacted, until some critical value whereupon fracture occurs. A Manson-Coffin relationship, as proposed by Stephenson and Nicholls [66] in modelling oxide erosion, seems appropriate.

In summary erosion mapping allows one to determine experimentally the boundary conditions for a given erosion damage mechanism, and thus the valid bounds for a particular erosion model. It should be noted that the erosion map, reproduced in Figure 15, was generated based on room temperature data/perceived erosion mechanisms operating at low to intermediate temperatures. The map can be applied at high temperatures provided the erosion mechanisms do not change significantly, nor do the mechanical properties of the ceramic top-coat, bondcoat or erodent particles. Under high temperature conditions, the map agrees well with impact damage caused by hard particles such as alumina, but is not valid for impacts by partially molten/pasty silica particles. This is associated with a change in material removal mechanism when an EB-PVD TBC is impacted by partially molten/pasty silica particles [47] for which a maximum in erosion rate is observed for 30º impacts.

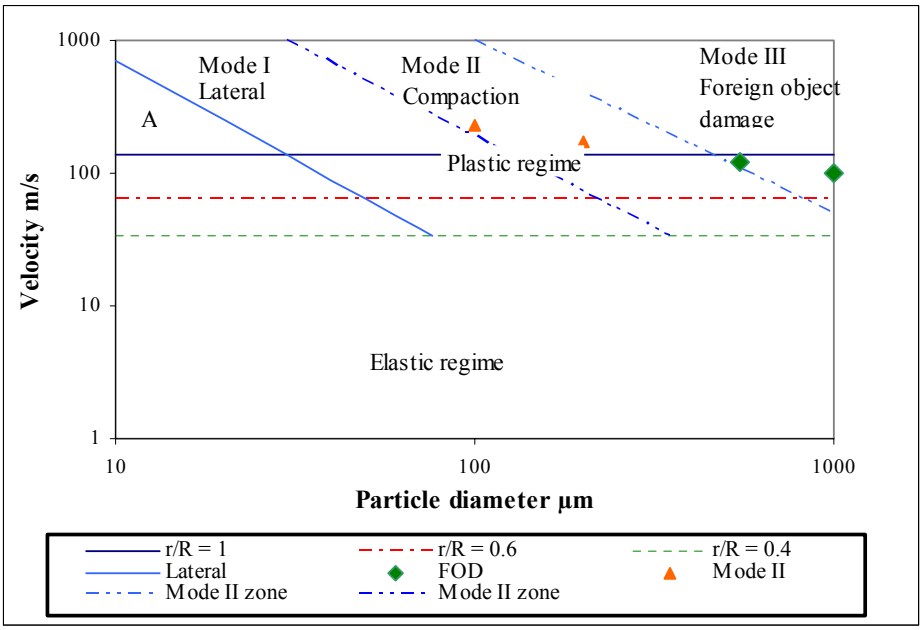

Figure 15 Erosion map for an EB-PVD thermal barrier coating eroded with silica Particles [57]

6.0 CONCLUSIONS

This paper has reviewed on-going research into the erosion and foreign object damage (FOD) to TBC systems. Both experiment and mathematical models (finite element analysis and Monté Carlo approaches) have been considered. As a result one can conclude that:

1) The impact of thermal barrier coatings by hard particles is a complex problem to solve. It requires a combination of experiment and mathematical models to understand the different interactions that may take place during particle impaction. These interactions depend on the flux, size and energetics of the particles. The morphology, structure and mechanical properties of the coating critically affects these impact processes and most importantly the temperature at which impact occurs as many of these properties are temperature dependent.

2) Experimental studies have shown that three primary damage regimes exist:-

Mode I : small particle erosion, whereby damage is limited to the near surface region of the TBC and material removal results from cracking of neighbouring columns during impact, usually at a depth of 10-20µm, and the conjoint loss of material from a cluster of adjacent columns. At high temperatures plastic deformation of the near surface region is observed and this defines the depth at which cracks propagate.

Mode II : compaction damage occurs when gross plasticity/densification is observed as a result of the impact event, but the induced stresses/strains are insufficient to induce fracture within the TBC. In effect the impact energy density falls below some critical threshold. This mode has the effect of

densifying the near surface of the coating, conditioning the TBC for later material removal due to small particle erosion or FOD.

Mode III : Foreign Object Damage (FOD). This is in effect a ballistic impact event. At its lower bound it may result in compaction damage, with possible lateral/shear crack development due to the large strains introduced during impaction. At its upper bound, extensive plasticity and densification occurs. Strain fields interact through the TBC and with the bondcoat and TGO. Under these conditions shear bands develop, propagating outward and down through the TBC, until they turn near the TGO interface to produce delamination cracks within the TBC ceramic, but parallel to the bondcoat/TGO/TBC interface. This is potentially the most damaging of the three mechanisms observed.

3) Finite element models have been developed to investigate each of these three regimes. These simulations concur with experimental observation and show that:

i) the small particle events, causing column cracking may be entirely elastic (for example at room temperature) or elastic/plastic. Elastic events operate on a time scale of 10-20ns and result in peak tensile stress 5-15μm below the TBC surface. Elastic/plastic interaction are of longer duration – upto 80-100ns – with failure concentrated at the elastic/plastic interface.

ii) increasing the particle size and impact energy of the particles leads to increased near surface plasticity and a lowering of the peak stresses that are generated. A threshold stress for column fracture, be it through column or by bending and shear band formation, is indicated. For impacts generating stress below this threshold only surface compaction will occur. Impact energies that exceed this threshold will result in cracking of the TBC columns adjacent to region of gross plastic damage.

iii) when the strain fields interact with the bondcoat/TGO/substrate interface delamination cracks may form. The extent of cracking is a function of the TBC ceramic thickness, its yield stress and fracture toughness.

4) Monté Carlo modelling methods have been implemented to integrate that damage mechanisms into an erosion life prediction model. The model has been coded for small particle erosion conditions – Mode I – to date and predicts erosion rates within ± 20% for a wide diversity of impact conditions that fall within the bounds of Mode I damage.

5) A preliminary erosion map has been devised that helps identify the various regimes (particle size, particle velocity etc) under which different erosion/FOD damage mechanisms may operate.

7.0 ACKNOWLEDGEMENTS

The authors wish to acknowledge the many sponsors that have supported this work. Particularly Rolls Royce plc for support of the early experimental erosion studies, the UK MoD and most recently the European Commission, through the joint NSF/EU HIPERCOAT programme contract no GRD2-200-30211.

REFERENCES

1) R. A. Miller "Current Status of TBCs – An Overview", Surface and Coating Technology 30, 1-11 (1987).

2) F. O. Soeching, "A Design Perspective on Thermal Barrier Coatings. In: Thermal Barrier Coating Workshop, NASA-CP_3312, p3-16, NASA, Cleveland (OH), (1995).

3) R. A. Miller "Thermal Barrier Coatings for Aircraft Engines – History and Directions, ibid. p17-34 (1995).

4) AGARD Report 823, "Thermal Barrier Coatings" AGARD Publications, Neuilly-Sur-Seine, France, (1998).

5) S. M. Meier and D. K. Gupta "The Evaluation of Thermal Barrier Coatings in Gas Turbine Engine Applications", Journal of Engineering for Gas Turbines and Power 116, 250-257, (1994).

6) T. E. Strangman 'Tailoring Zirconia Coatings for Performance in a Marine Gas Turbine Environment', Journal of Engineering for Gas Turbines and Power 112, (1990).

7) T. Cosack, L. Pawlowski, S. Schneidenbanger and S. Sturlese, "Thermal Barrier Coatings onto Turbine Blades by Plasma Spraying with Improved Cooling", ASME, J. Eng. Gas Turbine and Power, 116 272-276 (1994).

8) S. Sturlese and L. Bertamini, "Segmented Thermal Barrier Coatings on Turbine Blades and Diesel Engine Components" in 'Materials for Advanced Power Engineering;, Part 1, [Ed. Coutsouradis et al] 705-716, Kluwer Academic Pub, Netherlands (1994).

9) F. C. Toriz, A. B. Thakker and S. K. Gupta "Flight Service Evaluation of Thermal Barrier Coatings by Physical Vapour Deposition at 522 hours", Surface and Coating Technology 39/40, 161-172 (1989).

10) D. S. Rickerby and P. Morrell, Advantages/Disadvantages of various TBC systems as perceived by the Engine Manufacturer, AGARD-R0823, paper 20 (1998).

11) S. Alperine, M. Derrien, Y. Jaslier and R. Mevrel, "Thermal Barrier Coatings : The Thermal Conductivity Challenge", AGARD-R-833, paper 1 (1998).

12) R. A. Miller, 'Life Modelling of Thermal Barrier Coatings for Aircraft Gas Turbine Engines Hot Section' (eds. D. E. Sokolowski) NASA TM4087 (1989).

13) S. M. Meier, 'Thermal Barrier Coating Life Prediction Model Development' Journal of Engineering for Gas Turbines and Power, 114, (1992).

14) W. A. Nelson and R. N. Orenstein, "TBC Experience in Land Based Gas Turbines" in "Thermal Barrier Coating", NASA, p17- (1995).

15) R. F. Hanschuh, High Temperature Erosion of Plasma Sprayed Partially-Stabilised Zirconia in a Simulated Turbine Environment, NASA, TP2406 (Dec. 1984).

16) J. R. Nicholls, K. J. Lawson, D.S. Rickerby and P. Morrell, 'Advanced Processing of TBCs for Reduced Thermal Conductivity' Thermal Barrier Coatings AGARD Report 823, Paper 6 (1998).

17) D. Zhu, R. A. Miller, 'Thermal Conductivity and Sintering Behavior of Advanced Thermal Barrier Coatings', Ceram. Eng. Sci Proc 2002;23(4) 457-68.

18) J. R. Nicholls, K. J. Lawson, A. Johnstone, D. S. Rickerby, 'Methods to Reduce the Thermal Conductivity of EB-PVD TBCs' Surf. Coat. Technol. 2002;151-152:383-91.

19) M. J. Maloney, 'Thermal Barrier Coating Systems and Materials. In: US Patent 6 177200 Hartford (CT,USA), United Technology Corporation, 2001.

20) D. Zhu, J. a. Nesbitt, T. R. McCue, C. A. Barrett, R. A. Miller, ,Furnace Cylic Behavior of Plasma-Sprayed Zirconia-Yttria and Multi-component Rare Earth Oxide Doped Thermal Barrier Coatings', Ceram. Eng. Sci. Proc 2002, 23 (4), 533-45.

21) M. Watanabe, C. Mercer, C. G. Levi and A. G. Evans, Acta Materialia, 52 1479-1487, (2004).

22) J. R. Nicholls, 'Design of Oxidation-Resistant Coatings' JoM Paper, Vol. 52, Issue 1, Jan 2000 p28-35.

23) J. Stringer and r. Viswananthan 'Gas Turbine Hot Section Materials and Coatings in Electric Utility Applications' p1-21 Proc. ASM 'Materials Week' Pittsburg Penr (1993).

24) G. W. Goward, Surf. Coat. Technol. 108-109, 73- (1998)

25) J.R. Nicholls, 'Advances in Coating Design for High Performance Gas Turbines', MRS Bulletin 28 (9), 659-670 (2003).

26) T. A. Cruse, S. E. Stewart and M. Ortiz, "Thermal Barrier Coating Life Prediction Model Development' Transactions of the ASME, 110, 610-616 (1988).

27) B. C. Wu, E. Chang. S. F. Chang and C. H. Chao. "Thermal Cyclic Response of Yttria-Stabilised Zirconia/CoNiCrAlY Thermal Barrier Coatings", Thin Solid Films, 172, 185-196 (1989).

28) J. H. Sun, E. Chang, B. C. Wu, and C. H. Tsai. The Properties and Performance of (ZrO_2-8wt%Y_2O_3)/(CVD Al_2O_3) / (Ni-22wt%Cr-10wt%Al-1wt%Y) Thermal Barrier Coatings", Surface and Coatings Technology, 58, 93-99 (1993).

29) D. M. Nissley, "Thermal Barrier Coating Life Modelling in Aircraft Gas Turbine Engines", Thermal Barrier Coatings Workshop NASA-CP-3312, NASA Cleveland (OH) 265-281 (1995).

30) N. M. Yamar, G. M. Kim, F. S. Pettit and G. H. Meier in 'Turbine Forum' Nice, France (2002).

31) M. J. Steiger, N. M. Yanar, F. S. Pettit, G. H. Meier, 'Mechanisms of the Failure of Electron Beam Physical Vapour Deposited Thermal Barrier Coatings Induced by High Temperature Oxidation. In: Hampikian J. m. Dahotre, N. B. Editors. Elevated Temperature Coatings: Science and Technology III, Warrendale (PA): The Mineral, Metals and Materials Society, 199, p51-65.

32) M.F. Hussain and W. Tabakoff, "Dynamic Behaviour of Solid Particles Suspended by Polluted Flow in a Turbine Stage", Journal of Aircraft 10, 434-440 (1973).

33) R. A. Wenglarz and W. Tabakoff, J. Test Eval. 10, 298-302, (1982).

34) J. E. Facknall, Wear 134, 237-252 (1989).

35) W. Tabakoff, A. Hamed and B. Beacher 'Investigation of Gas Particle Flow in an Erosion Wind Tunnel", Wear 86, 73-88 (1983).

36) D. Günes and M. Mengütürk "Improved Particle Trajectory Calculation Around a Blade Leading Edge", Proc. 6th Int. Conf. on "Erosion by Liquid and Solid Impact, p52, [Eds J. E. Field and N. S. Corney] Cavendish Laboratory, Cambridge, UK (1983).

37) R.E.Restall & D. J. Stephenson, J. Mater. Sci. Eng. 88, 273-282, (1987)

38) R. G. Wellman and J. R. Nicholls, Some Observations on the Erosion Mechanism of EB-PVD TBCs. Wear 242, 89-96 (2000).

39) R.G. Wellman and J. R. Nicholls, "Observed Damage Mechanisms in the Erosion and FOD of EB-PVD TBCs", accepted for publication in Wear (2004)

40) W. Tabakoff 'Investigation of Coatings at High Temperature for Use in Turbomachinery", Surface and Coatings Technology, 39/40, 97-115 (1989).

41) J. R. Nicholls, M. J. Deakin and D. S. Rickerby, "A Comparison Between the Erosion Behaviour of Thermal Spray and EB-PVD Thermal Barrier Coatings", Wear 233-235 (1999) p352-361.

42) J. R. Nicholls, Mater. at High Temp. 14(3), 289-306 (1997).

43) T. Rhys-Jones and C. F. Toriz ,"Thermal Barrier Coatings for Turbine Applications in Aero Engines", High Temperature Technology 7, (1989).

44) A. G. Davis, D.H. Boone and A. V. Levy , "Erosion of Ceramic Thermal Barrier Coatings", Wear 110, 101-116 (1986).

45) H. E. Eaton and R. G. Novak "Particulate Erosion of Plasma-Sprayed Porous Ceramic", Surface and Coatings Technology, 30, 41-50 (1987).

46) M. R. Dorfman and J. D. Reardon, "Advanced Thermal Barrier Coating Systems", NASA TBC Workshop, May 1985.

47) J. R. Nicholls, Y. Jaslier and D. S. Rickerby, "Erosion and Foreign Object Damage of Thermal Barrier coatings", Materials Science Forum, Vol;. 251, No pt1-2 pp935-948, 1997.

48) J. R. Nicholls, Y. Jaslier and D. S. Rickerby, "Erosion of EB-PVD Thermal Barrier Coatings, "Materials at High Temperatures, 15 (1) 15-22, (1998).

49) R. G. Wellman and J. R. Nicholls, "A Mechanism for the Erosion of EB-PVD TBCs, Materials Science Forum 369-372, 531-538 (2001).

50) R.G. Wellman and J. R. Nicholls, "A Monté Carlo Model for Predicting the Erosion Rate of EB-PVD TBCs, Wear 256, 889-899, (2004).

51) J. R. Nicholls, R. G. Wellman and M. J. Deakin, "Erosion of Thermal Barrier Coatings", Materials at High Temperatures 20, 207-218, (2003).

52) R. G. Wellman and J. R. Nicholls, 'Workshop on Thermal Barrier Coatings' Paris, France, Aug (2003).

53) X. Chen, J. W. Hutchinson and A. G. Evans, 'Simulation of the High Temperature Impression of Thermal Barrier Coatings with Columnar Microstructure' Acta. Materialia 52 565-571 (2004).

54) X. Chen, R. Wang, N. Yao, A. G.Evans, J. W. Hutchinson and R. W. Bruce, Materials Science and Engineering A (2002), in press.

55) X. Chen, M. Y. He, I. Spitsberg, N. A. Fleck, J. W. Hutchinson and A. G. Evans, 'Mechanisms Governing the High Temperature Erosion of Thermal Barrier Coatings' Wear 256, 735-746 (2004).

56) N. A. Fleck, Presented at the 'Thermal Barrier Coating Workshop', Santa Barbara USA, Jan 2004.

57) R.,G. Welllman, M. J. Deakin and J. R. Nicholls, 'Effect of TBC Morphology on the Erosion Rate of EB-PVD TBCs.

58) R. G. Wellman, J. R. Nicholls and A. Dyer, 'Nano and Micro Indentation of Bulk Zirconia and EB-PVD TBCs', Surface Coatings and Technology 176 253-260, (2004).

59) X. Chen and J. W. Hutchinson, J. Mech. Phys. Solidus, 50, 2669-2690 (2002).

60) B.R. Lawn and A. G. Evans, J. Mat. Sci 12 2195-2201 (1977).

61) B. R. Lawn, D. B. Marshall and A. G. Evans, J. Am. Ceram. Soc. 63, 574-580 (1980).

62) B. R. Lawn, 'Fracture of Brittle Solids', Cambridge University Press (1993).

63) M. A. Verspui, G. deWith, A. Corbijn and P. J. Slikkerveer, 'Simulation Model for Erosion of Brittle Materials', Wear 233-235, 436-44 (1999).

64) S.S. Chang, D. B. Marshall and A. G. Evans, 'The Response of Solids to Elastic/Plastic Indentation, Stresses and Residual Stresses', J. Applied Phys. 53 298-311 (1982).

65) R. Hill 'Plasticity', Oxford University Press, Oxford (1950).

66) D. J. Stephenson and J. R. Nicholls 'Modelling the Influence of Surface Oxidation on High Temperature Erosive Wear' Wear 186-187, 284- (1995).

AVT-109
Specialist Meeting on the Control and Reduction of Wear in Military Platforms

Summary of Discussion Sessions

The following presents a summary of the discussion of papers presented in the various sessions of the workshop. Only questions where the authors provided transcripts of their answers are reported.

Session 4 – Gas Turbine Wear and Erosion
Chair: Dr. Mike Winstone, DSTL, UK

Paper MP-AVT-109-20

Major M. Colvita, Italian Air Force, Italy

Q. Pre-fragmentation on plasma sprayed coatings, does it affect their performance with respect to the corrosion aspects?

Prof. John Nicholls, Cranfield University, UK

A. Pre-cracking of an APS or HVOF coating is achieve during coating deposition (by rapidly quenching during deposition). The coating cracking does not appear to influence bondcoat oxidation. However, in vanadium fuels, corrosion of the ceramic can occur down the cracks, due to vanadium reacting with yttria in the TBC. This destabilizes the ceramic and can lead to ceramic spalling.

Dr. Prakash Patnaik, NRC-IAR, Canada.

Q. You mentioned about the 'prime reliance' focus for thermal barrier coatings. Could the bondcoat not be responsible as well?

Prof. John Nicholls, Cranfield University, UK

A. TBCs are a very complex system, currently bondcoat oxidation is life limiting. Erosion and FOD are secondary, but important factors. If the TBC thins (erosion) then the temperature of the bondcoat/TBC interface increases exacerbating bondcoat oxidation. FOD, or more precisely multiple FOD impacts can remove TBC down to near the bondcoat/TBC interface.

Dr. Prakash Patnaik, NRC-IAR, Canada

Q. What are the high temperature affects on foreign object damage?

Prof. John Nicholls, Cranfield University, UK

A. We believe that above 800ºC, there is sufficient plasticity in the TBC ceramic to provide a representative damage mode from FOD. One must however, bear in mind that particle properties can also change with increase in temperature.

Dr. Prakash Patnaik, NRC-IAR, Canada

Q. What are your comments on the erosion performance of zig-zag TBC microstructures?

Prof. John Nicholls, Cranfield University, UK

A. My belief is that zig-zag microstructures will have poor erosion resistance. I have offered to test such structured coatings, but have not been sent any to test yet.